

# Random lattice strain and its relaxation towards the morphotropic phase boundary of $\text{Na}_{0.5}\text{Bi}_{0.5}\text{TiO}_3$ -based piezoelectrics: Impact on the structural and ferroelectric properties

Gobinda Das Adhikary,<sup>1</sup> Dipak Kumar Khatua,<sup>1</sup> Anatoliy Senyshyn,<sup>2</sup> and Rajeev Ranjan<sup>1,\*</sup>

<sup>1</sup>Department of Materials Engineering, Indian Institute of Science, Bangalore-560012, India

<sup>2</sup>Forschungsmaterialienquelle Heinz Maier-Leibnitz (FRM II), Technische Universität München, Lichtenbergstrasse 1, D-85747 Garching b. München, Germany



(Received 31 January 2019; revised manuscript received 23 April 2019; published 29 May 2019)

We demonstrate that the lead-free piezoelectric compound  $\text{Na}_{0.5}\text{Bi}_{0.5}\text{TiO}_3$  (NBT) exhibits random lattice strain in the ferroelectric phase, and that this feature primarily dictates the way the system evolves towards the morphotropic phase boundary in the unpoled state of NBT-based piezoelectrics. Investigations on two different morphotropic phase boundary (MPB) systems, namely  $\text{Na}_{0.5}\text{Bi}_{0.5}\text{TiO}_3 - \text{K}_{0.5}\text{Bi}_{0.5}\text{TiO}_3$  (NBT-KBT) and  $\text{Na}_{0.5}\text{Bi}_{0.5}\text{TiO}_3 - \text{BaTiO}_3$  (NBT-BT), revealed that the coupled structural-polar evolution towards the MPB is primarily driven by the necessity to minimize this strain. Our study suggests that the random lattice strain originates in the random stacking of the in-phase tilt and antiphase octahedral tilted regions, and that the system is able to minimize it by adopting a sequential stacking of the two tilt types, leading to a long-period modulation in the octahedral tilt configuration over large parts of the sample volume. This hinders the development of long-range ferroelectric order as the MPB is approached. We also demonstrate that the composition showing the maximum piezoelectric coefficient corresponds to a structural state wherein considerable polar-structural disorder coexists with the field-stabilized long-range rhombohedral ferroelectric order after poling, and not coexistence of two ferroelectric phases (tetragonal and rhombohedral), generally believed.

DOI: [10.1103/PhysRevB.99.174112](https://doi.org/10.1103/PhysRevB.99.174112)

## I. INTRODUCTION

High-performance  $\text{ABO}_3$  ferroelectric perovskites are used as actuators, pressure sensors, and transducers in wide-ranging applications spanning sectors like health, space, defense, and automobiles [1,2]. For over four decades,  $\text{Pb}(\text{Zr}_x\text{Ti}_{1-x})\text{O}_3$ , commonly known as PZT, has been the preferred choice for such applications. The composition-temperature phase diagram of PZT exhibits a morphotropic phase boundary (MPB) which separates ferroelectric tetragonal (space group  $P4mm$ ) phase field from a ferroelectric rhombohedral (space group  $R3m$ ) phase field at  $x = 0.52$  [3]. The interferroelectric instability at the MPB enables intrinsic and extrinsic mechanisms which enhance the electromechanical response of the system [4–8]. Increased environmental concerns and directives in the last decade and a half [9,10] have led to a great thrust in research on developing lead-free alternatives of PZT [11]. This endeavor has led to extensive studies on  $\text{BaTiO}_3$ -based [12–21],  $(\text{K}, \text{Na})\text{NbO}_3$ -based [22–25], and  $\text{Na}_{0.5}\text{Bi}_{0.5}\text{TiO}_3$ -based [26–31] ferroelectrics. Guided primarily by the PZT experience, the choice of alloying element(s) in these systems was motivated by driving the system towards an interferroelectric instability. In the case of  $\text{BaTiO}_3$ -based systems the three important alloying elements which could do the job are Zr, Sn, and Hf [32]. The highest piezoelectric response in  $\text{BaTiO}_3$ -based systems is achieved at the tetragonal ( $P4mm$ )-orthorhombic ( $Amm2$ ) phase boundary [12,13,16,17,32]. The same scenario is reported in

KNN-based systems wherein the interferroelectric instability is achieved at room temperature by Li, and Sb modifications [22,24,33]. The most investigated solid solutions of the NBT-based ferroelectrics are  $(\text{Na}_{1-x}\text{K}_x)_{0.5}\text{Bi}_{0.5}\text{TiO}_3$  (NBT-KBT) and  $(\text{Na}_{0.5}\text{Bi}_{0.5})_{1-x}\text{Ba}_x\text{TiO}_3$  (NBT-BT). Both  $\text{BaTiO}_3$  and  $\text{K}_{0.5}\text{Bi}_{0.5}\text{TiO}_3$  are tetragonal ( $P4mm$ ) ferroelectrics which when dissolved in the matrix of NBT are anticipated to induce a rhombohedral-tetragonal interferroelectric instability. It is important to note that among the three important lead-free ferroelectric compounds BT, KNN and NBT, the first two (BT and KNN) belong to the category of normal ferroelectrics. NBT, on the other hand, belongs to the category of relaxor ferroelectrics, characterized by strong structural-polar disorder on the nanoscale [34,35]. This disorder is expected to play an important role in determining the structural, dielectric, and piezoelectric properties of the NBT-based piezoelectrics as the MPB is approached. This aspect has received less attention in literature so far.

The first symptom of local structural disorder in NBT was reported by Kreisel *et al.*, who, based on a diffuse x-ray scattering study, suggested local monoclinic displacement of the A-site cations in NBT [36] in the otherwise global rhombohedral ( $R3c$ ) symmetry. Electron-diffraction studies have revealed thin sheets of localized in-phase (+) tilted octahedral regions (Glazer's notation:  $a^0a^0c^+$ )—a residue of the high-temperature  $P4bm$  phase [37]. Levin and Reaney argued that the assemblage of the in-phase and the antiphase tilted regions gives rise to an average monoclinic ( $Cc$ ) structure [38], reported earlier by Aksel *et al.* [39] and Gorfman *et al.* [40]. Balagurov *et al.*, on the other hand, have reported that the combination of  $a^0a^0c^+$  and  $a^-a^-a^-$  gives rise to a long-period

\*rajeev@iisc.ac.in

structural modulation [41]. The signature of the long-period modulation was observed in neutron diffuse scattering [41], and not in the regular powder-diffraction patterns, suggesting its short correlation length. Strong electric field (i) reorients the *A*-site cations towards the rhombohedral compatible [111] direction [35,42]; (ii) suppresses the local in-phase ( $a^0a^0c^+$ ) tilted regions [34]; and (iii) transforms the monoclinic (*Cc*) structure to rhombohedral (*R3c*) on the global scale [34,43].

Following the conventional approach, the first phase diagram of NBT-BT by Takenaka *et al.* [44] shows the MPB in NBT-BT as a boundary separating rhombohedral and tetragonal phase regions. Later studies reported a cubiclike phase of the MPB composition,  $0.94\text{NBT} - 0.06\text{BaTiO}_3$  [45]. Neutron powder diffraction of this composition revealed weak superlattice reflections which cannot be explained based on the simple octahedral tilt models [28]. Analogous to NBT-BT, the composition ( $x = 0.20$ ) exhibiting the maximum piezoelectric response in  $\text{NBT} - x\text{KBT}$  [46,47] has also been reported to exhibit a cubiclike phase [26,48]. Levin *et al.* have rationalized that  $x = 0.20$  of NBT-KBT does have local tetragonal and rhombohedral ferroelectric regions [26]. At the same time some studies have indicated that the propensity of the in-phase tilted regions grows considerably at the MPB [26,29,34,38,49]. Two scenarios can be envisioned when the volume fraction of the local in-phase tilted regions grows: (i) the two tilt types compete and increase the structural frustration of the system, or (ii) they start to collaborate/cooperate and exhibit long-period modulation [41] throughout the sample volume. However, the fundamental question is why should the system show enhanced propensity for in-phase tilted regions, which is not conducive for the development of ferroelectric order, as the MPB is approached?

The increased propensity for the in-phase tilt as the system heads for an interferroelectric instability will greatly affect its structural-polar state and thereby the weak-field properties such as the relative permittivity (of the unpoled specimens). Unlike the measurement of relative permittivity which can be performed on unpoled specimens, piezoelectric measurements necessarily involve first subjecting the system to strong electric field, i.e., poling. It is therefore important to relate the piezoelectric response to the structural-polar states of poled specimens, and the dielectric response of unpoled specimens to the structural-polar state of the unpoled specimens. Structural analysis of poled specimens also helps in ascertaining the ground-state structure of relaxor ferroelectric systems which do not exhibit long-range structural order in the absence of electric field. Electric field can increase the correlation length of the ferroelectric phase and reveal the nature of the noncubic ferroelectric ground-state structure using common techniques such as x-ray diffraction (XRD). This was recently demonstrated for a relaxor ferroelectric-based pseudoternary system  $\text{BiFeO}_3 - \text{PbTiO}_3 - \text{LaFeO}_3$  exhibiting very large electrostrain [50] wherein the local structure of what appears to be cubic phase on the global scale was proven to be tetragonal. For normal MPB ferroelectric such as  $\text{PbTiO}_3 - \text{BiScO}_3$  [51] and  $\text{PbTiO}_3 - \text{PbZrO}_3$  [52] this approach may not be required since the structure of the coexisting ferroelectric phases is easily revealed on the global scale even in the unpoled state; poling retains the two-phase state in these systems [51]. Using x-ray total scattering, Goetzee-Barral *et al.* have shown

a field-driven ordering in the Bi-Ti cation-cation distances for the MPB compositions of NBT-KBT [53]. Zeng *et al.* suggested that the high piezoelectric response of perovskite ferroelectric ceramics stems from poling field induced ordered nanodomains for NBT-BT systems [54]. While these studies are important indicators that poling induces structural changes on the local and nanometer length scales, a systematic one-to-one correspondence of the structure of the poled state with the piezoelectric response is still missing. In this paper we examine the coupled structural-polar evolution of the  $(1-x)\text{NBT}-(x)\text{KBT}$  system using a variety of complementary techniques namely x-ray diffraction, neutron powder diffraction (NPD), Raman spectroscopy, and dielectric measurements. Our study reveals: (i) the existence of random lattice strain in the parent compound NBT in its virgin (unpoled) state; (ii) the evolution towards the MPB is dictated by the necessity to minimize this strain by collaborative coupling between the antiphase and in-phase octahedral tilts; and (iii) the composition  $x = 0.20$  exhibiting maximum piezoelectric response does not exhibit coexistence of two ferroelectric phase in the poled state, but rather a coexistence of long-range ferroelectric and disordered phases.

## II. EXPERIMENTAL

Ceramic specimens  $(1-x)\text{Na}_{0.5}\text{Bi}_{0.5}\text{TiO}_3 - (x)\text{K}_{0.5}\text{Bi}_{0.5}\text{TiO}_3$  (NBT-*x*KBT) were prepared using the conventional solid-state route. Dried powders of  $\text{Na}_2\text{CO}_3$  (99.5%, Alfa Aesar),  $\text{K}_2\text{CO}_3$  (99%, Alfa Aesar),  $\text{Bi}_2\text{O}_3$  (99%, Alfa Aesar), and  $\text{TiO}_2$  (99.8%, Alfa Aesar) were taken in stoichiometric ratios and mixed in an acetone medium using zirconia vials and balls in a planetary ball mill at 150 rpm for 12 h. Milled powders were dried, ground, and calcined at 900 °C for 3 h in covered alumina crucibles. The calcined powders were remilled at 150 rpm for 8 h. The ceramic composition of  $(1-y)\text{Na}_{0.5}\text{Bi}_{0.5}\text{TiO}_3 - (y)\text{BaTiO}_3$  (NBT-*y*BT) was also prepared following the same synthesis route. Dried remilled powders were mixed with 5% poly vinyl alcohol (PVA) and then pressed into pellets under uniaxial pressure of 100 MPa followed by cold isotropic pressure of 300 MPa. Green pellets were sintered in covered alumina crucibles at 1150 °C for 4 h in air. Density measurement of sintered pellets carried out using liquid displacement method showed average density  $\sim 95\%$  of the theoretical density. The sintered pellets with diameters of 10–12 mm and thickness of 0.8–1.5 mm were painted with silver paste for electrical contact and were poled by applying a dc field in the range of 50–70 kV/cm for 30 min. Direct piezoelectric coefficient ( $d_{33}$ ) of poled pellet was measured using Piezotest, PM300 with applied force 0.25 N and frequency 110 Hz. X-ray powder diffraction was carried out using a Rigaku Smartlab x-ray diffractometer with monochromatic  $\text{Cu K}\alpha_1$  radiation. Raman spectra were collected from poled and unpoled pellets using 532 nm laser attached with LabRAM HR (HORIBA) spectrometer. X-ray powder diffraction (XRPD) of the poled specimens was obtained after crushing the poled pellets gently to powder. The XRPD patterns of the unpoled specimens were collected after annealing the powder at 750 °C for 2 h obtained after crushing the sintered pellets to remove the effect of residual stress incurred during the

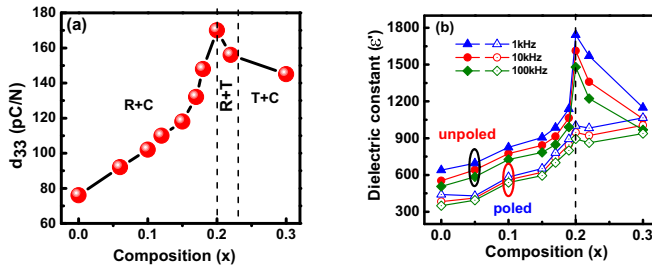


FIG. 1. Composition dependence of (a) longitudinal piezoelectric coefficient ( $d_{33}$ ) and (b) dielectric constant ( $\epsilon'$ ) of both unpoled and poled NBT –  $x$ KBT specimens.

grinding process. Neutron powder-diffraction data were collected at the diffractometer SPODI at FRM-II, Germany (wavelength of 1.548150 Å) [55]. Structural analysis was performed by the Rietveld method using the FULLPROF package [56].

### III. RESULTS

#### A. Dielectric and piezoelectric behavior

Figure 1(a) shows the composition ( $x$ ) dependence of the weak-field longitudinal piezoelectric coefficient ( $d_{33}$ ) of NBT –  $x$ KBT. A peak at  $x = 0.20$  confirms this composition to be the critical MPB composition in conformity with the earlier reports [26,46]. The composition dependence of relative permittivity of the unpoled specimens also shows a sharp peak at  $x = 0.20$  [Fig. 1(b)]. The permittivity is reduced after poling for all compositions; the maximum reduction occurs for  $x = 0.20$ . In contrast to the unpoled specimens, the poled specimens do not show a sharp maximum in the composition dependence of permittivity at  $x = 0.20$ . After a slight decrease at  $x = 0.22$ , the permittivity of the poled compositions increases gradually with composition. For example, the relative permittivity of  $x = 0.30$  is slightly larger than that of  $x = 0.20$  although the piezoelectric constant ( $d_{33}$ ) shows a decreasing trend [Fig. 1(a)]. This suggests a lack of intimate correlation between the dielectric and piezoelectric behavior in poled specimens. This result also highlights the importance to differentiate the structure-property correlations between poled and unpoled specimens in such systems.

A less-explored property is dielectric dispersion (frequency variation of the relative permittivity) and its use as a tool to investigate the degree of polar heterogeneity in piezoceramics. NBT and its derivatives belong to the family of relaxor ferroelectrics and exhibit polar nanoregions (of varying sizes). This is expected to impart a great degree of polar heterogeneity and thereby affect the dispersion behavior of the system. A recent report by Groszewicz *et al.* [57] seems to support this viewpoint. Investigating the NBT-BT system, the authors show that compositions exhibiting long-range ferroelectric order show reduced dispersion (permittivity difference,  $\Delta\epsilon$ , measured at two different frequencies) as compared to the compositions exhibiting features of a relaxor ferroelectric [57]. The degree of dielectric dispersion can therefore be judiciously used as a parameter to get a sense of the degree of polar heterogeneity in NBT-based ferroelectrics [28]. Since long-range

ferroelectric state can also be stabilized in the nonergodic relaxor ferroelectric state by application of strong electric field, we anticipate the reduction in dielectric dispersion by the poling field. A comparison of the dielectric dispersion before and after poling for the different compositions can shed light on the role of polar heterogeneity in influencing the piezoelectric response of the critical composition ( $x = 0.20$ ) of the NBT-KBT system.

Figures 2(a) and 2(b) shows the frequency (on the logarithmic scale) versus relative permittivity in the unpoled and poled states of two representative compositions  $x = 0.00$  and  $x = 0.20$ . The linear curves allow us to use the slope ( $s$ ) as a measure of the degree of dispersion. The composition variation of the slope, shown in Fig. 2(c), reveals that for any given composition, the permittivity dispersion is reduced after poling. Both the unpoled and poled specimens separately show enhanced dielectric dispersion on approaching  $x = 0.20$ . This implies that the critical composition,  $x = 0.20$ , showing maximum  $d_{33}$  retains a considerable degree of polar heterogeneity even after poling. The difference in the slopes,  $\Delta s$ , before and after poling can be considered as a quantitative measure of the suppression of the polar heterogeneity by the poling field. Interestingly, this parameter is also considerably enhanced on approaching the critical composition  $x = 0.20$  [Fig. 2(d)]. That is,  $x = 0.20$  happens to be composition which not only shows significantly enhanced polar heterogeneity in the unpoled state, but also its maximum suppression by the poling field [Fig. 2(d)]. Yet, the poled  $x = 0.20$  retains considerable polar heterogeneity, comparable to what is present in the unpoled compositions of  $x < 0.20$ . A correlation between piezoelectric response and the polar heterogeneity is depicted in Fig. 2(e).

#### B. Global structures in the unpoled state

Figure 3 shows the evolution of the three characteristic pseudocubic x-ray Bragg profiles with composition of unpoled and poled NBT-KBT. The triplet nature of the pseudocubic  $\{110\}_{pc}$ , with the two side peaks nearly half the intensity of the middle peak, suggests a monoclinic average structure of unpoled  $x = 0$ , i.e., pure NBT [39]. With increasing  $x$ , this splitting gradually disappears. Consistent with the previous reports [34,39] the XRD patterns of unpoled  $x = 0.20$  and  $x = 0.22$  suggest a cubiclike structure. Concomitantly, the superlattice reflection at  $2\theta = 38.46^\circ$  characteristic of the rhombohedral ( $R3c$ ) phase becomes invisible for  $x \geq 0.20$ . While the XRD pattern of unpoled  $x = 0$  (NBT) required monoclinic ( $Cc$ ) model for a satisfactory Rietveld fitting, it was possible to fit the XRD patterns of unpoled  $0.06 \leq x \leq 0.18$  satisfactorily with  $R3c + Pm-3m$  structural model. The XRD patterns of unpoled  $x = 0.20$  and  $x = 0.22$  can be satisfactorily fit with single-phase cubic ( $Pm-3m$ ) structural model [Fig. 4(a)]. The composition dependence of the cubic phase fraction shows a sharp rise just before  $x = 0.20$  [Fig. 4(b)]. This correlates very well with the sharp maximum at  $x = 0.20$  in the permittivity of the unpoled specimens [Fig. 1(b)].

We also found an interesting trend in the composition dependence of the full width at half maximum (FWHM) of the  $\{200\}_{pc}$ . The  $\{200\}_{pc}$  profile is singlet for all unpoled

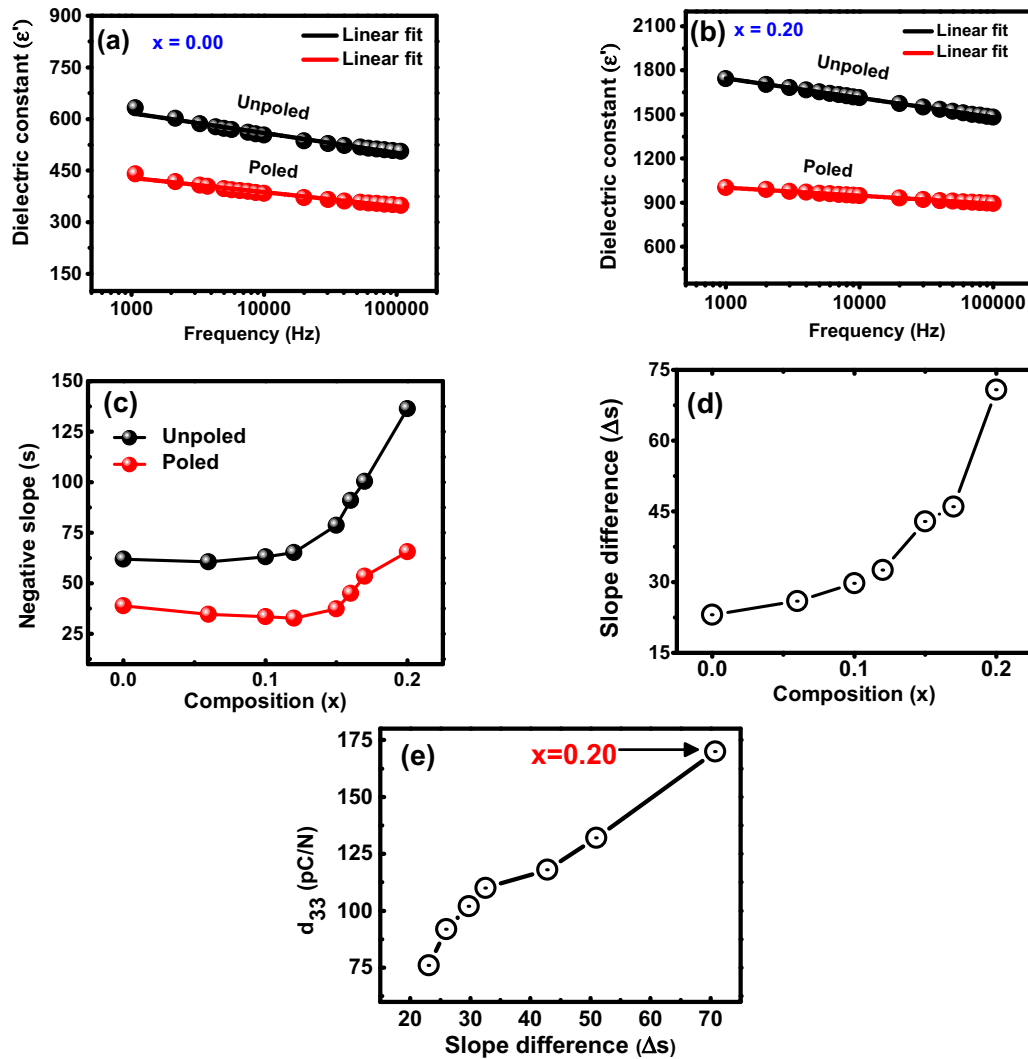


FIG. 2. Frequency dependence of dielectric constant of unpoled and poled (a) NBT and (b) NBT-0.20KBT. (c) Composition dependence of the negative slope ( $s$ ) obtained from the dielectric dispersion plots of the different compositions before and after poling. The composition dependence of the slope difference ( $\Delta s$ ) before and after poling is shown in (d). A correlation between piezoelectric coefficient ( $d_{33}$ ) and  $\Delta s$  is shown in (e).

compositions  $x \leq 0.22$ , irrespective of whether the average structure appears as monoclinic  $Cc$ , rhombohedral  $R3c$ , or cubic. The FWHM of this peak can be seen to decrease systematically for  $x > 0.10$  with the value reaching a minimum (close to the experimental resolution of the diffractometer) at  $x = 0.20$  [Fig. 4(b)]. We may clarify that this systematic decrease in FWHM cannot be attributed to the grain-size effect as all compositions show grains in the range of few microns (Fig. 5). The additional broadening of the pseudocubic  $\{200\}_{pc}$  of unpoled NBT suggests the existence of inhomogeneous/random lattice strain. KBT substitution gradually relaxes this strain and minimizes it at  $x = 0.20$ . We also examined this phenomenon in the other MPB system NBT -  $y$ BT and found a similar trend in composition dependence of the FWHM of  $\{200\}_{pc}$  of the unpoled specimens (Fig. 6). This confirms that the MPB in both NBT-KBT and NBT-BT is associated with the minimization of the inhomogeneous/random lattice strain the system inherited from its parent compound NBT.

### C. Collaborative coupling of the octahedral tilts in unpoled specimens

Very recently we have shown that the neutron powder-diffraction pattern of the MPB composition of unpoled NBT-KBT and NBT-BT suggests long-period modulation in the octahedral tilt configuration [29,58]. For ready reference, we show this feature again in Fig. 7, both for the NBT-0.20KBT and NBT-0.06BT. In contrast to the XRD, the NPD patterns of the MPB compositions of both the systems show weak superlattice reflections. The weak superlattice reflections in both the cases appear at the same  $d$  spacings suggesting that they owe their origin to a similar structural (octahedral) distortion. A Le Bail fit of the NPD pattern [Fig. 7(a)] with  $2 \times 2 \times 2$  cubic supercell fails to account accurately for the superlattice reflections. For example, a close observation revealed that the calculated positions of superlattice reflections are unable to match accurately the observed peak positions. For example, the superlattice profile

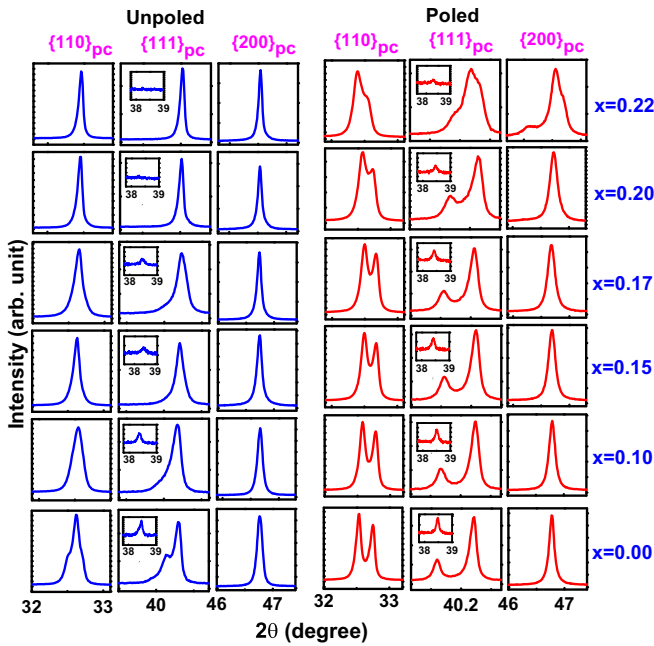


FIG. 3. Composition evolution of three selected pseudocubic x-ray powder-diffraction Bragg profiles  $\{110\}_{pc}$ ,  $\{111\}_{pc}$ , and  $\{200\}_{pc}$  of unpoled and poled NBT- $x$ KBT specimens. The insets highlight position of  $1/2\{311\}_{pc}$  superlattice reflection. The superlattice reflection becomes visible after poling for  $x = 0.20$  and  $x = 0.22$ . The split pattern of the Bragg profiles of poled  $x = 0.20$  suggests rhombohedral ( $R3c$ ) structure whereas that of  $x = 0.22$  suggest rhombohedral ( $R3c$ )+tetragonal ( $P4mm$ ) structure.

near  $2\theta \sim 51^\circ$  exhibits a doublet with peaks at  $51.2^\circ$  and  $51.5^\circ$ , respectively. The full profile decomposition, on the

other hand, predicts a peak only at  $51.2^\circ$ , corresponding to the  $R3c$  phase. The peak at  $51.5^\circ$  remains unaccounted for. Another example of the unsatisfactory fit can be noticed near  $2\theta \sim 72^\circ$ . Here the observed superlattice peak occurs at  $72.05^\circ$  whereas the calculated superlattice peak is at  $71.8^\circ$ . Another notable discrepancy is detected near  $99.5^\circ$  in terms of a peak [shown by arrow in Fig. 7(a)] which is completely unaccounted for. This analysis confirms that the set of superlattice peaks observed in the NPD of the unpoled MPB composition is not due to simple octahedral tilts (in the framework of Glazer's tilt systems [59]). A bigger supercell is needed to account for the misfits shown above. In search for the smallest volume long-period modulated cell, we searched for the best fit with supercells of the type  $\sqrt{2}a \times \sqrt{2}a \times na$  (Fig. 8) and found that the minimum value  $n$  which could index all the peaks satisfactorily to be 10. Interestingly this periodicity is the same as reported earlier in pure NBT by Thomas *et al.* [60] and confirms that the MPB compositions of both NBT-KBT and NBT-BT is characterized by the long-period modulation of the octahedral tilt throughout the sample volume. The relaxation of the inhomogeneous/random lattice strain, shown above in Sec. III B, appears to be intimately related to this phenomenon.

#### D. Global structures in the poled state

Irrespective of the structural states (cubic or monoclinic/rhombohedral) of the unpoled specimens, poling irreversibly transforms all the compositions in the range  $x \leq 0.20$  to rhombohedral as evident from the characteristic splitting of the pseudocubic  $\{110\}_{pc}$  and  $\{111\}_{pc}$  into two and the singlet nature of  $\{200\}_{pc}$  (Fig. 3). Keeping in view the fact that mechanical stress also changes the average structure of NBT-based piezoelectrics [27], the confirmation that the

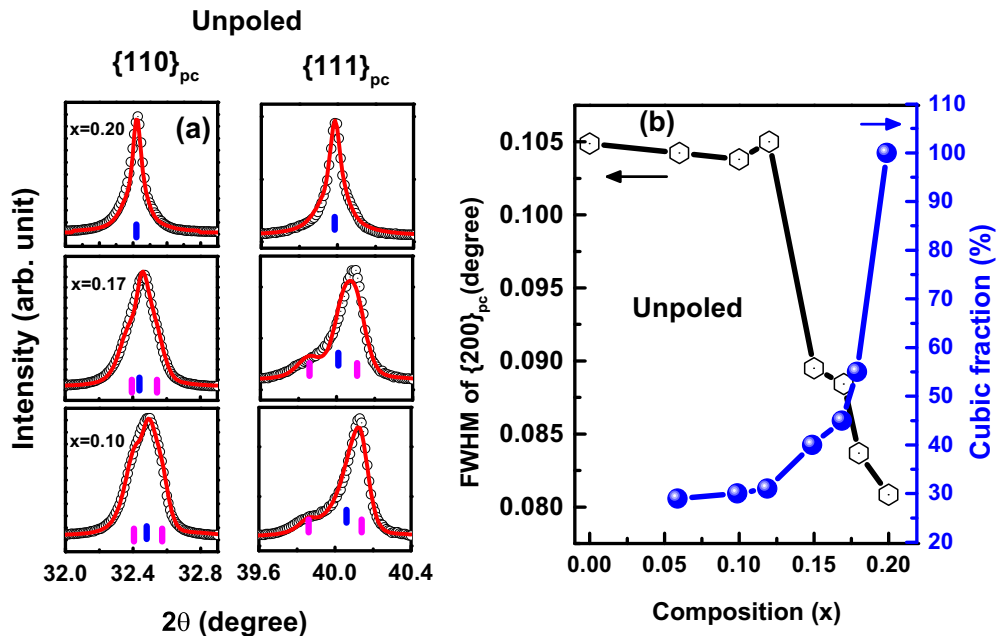


FIG. 4. (a) Rietveld refinement with  $R3c + Pm-3m$  structures for  $0.06 \leq x \leq 0.18$  compositions and with  $Pm-3m$  structure for  $x = 0.20$  composition. (b) Composition dependence of the FWHM of the singlet Bragg profile  $\{200\}_{pc}$  of unpoled NBT- $x$ KBT and variation of cubic phase fraction of unpoled specimens with compositions ( $x$ ).

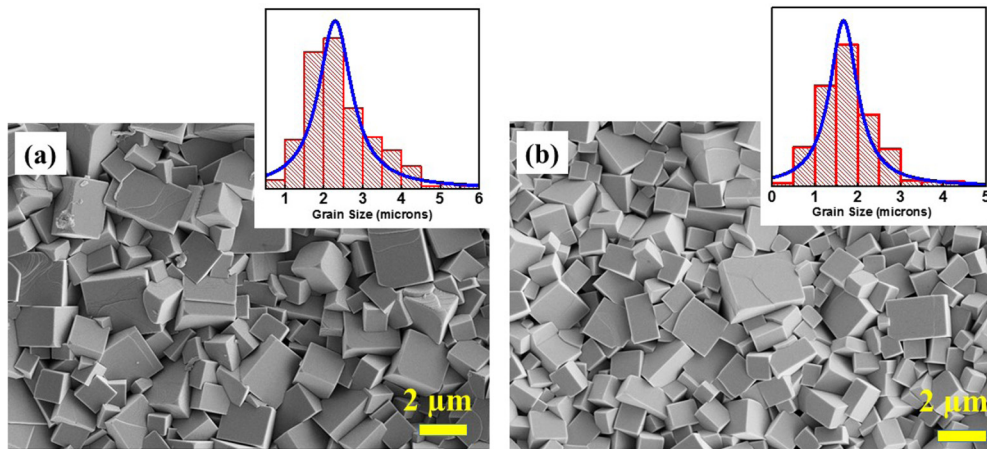


FIG. 5. Scanning electron microscope micrographs of  $x = 0.10$  (a) and  $x = 0.20$  (b) compositions of NBT –  $x$ KBT system with histograms of grain/particle size distribution in the insets of the figure.

poling field transforms the cubiclike phase of  $x = 0.20$  to rhombohedral was doubly confirmed by performing XRD measurements on a poled pellet of  $x = 0.20$  (Fig. 9). The splitting of  $\{111\}_{pc}$  profile after poling into two confirms the poling-induced cubic to rhombohedral transformation in the pellet. The higher intensity ratio of the peak on the left as compared to that on the right of the doublet is due to poling-induced preferred orientation in the pellet specimen. The preferred orientation is removed after the poled pellet is ground to powder while the grains retain the structural changes (cubic to rhombohedral) induced by the poling field (Fig. 9). The composition  $x = 0.22$ , which similar to  $x = 0.20$  appears cubic in the unpoled state, exhibits coexistence of rhombohedral ( $R3c$ ) and tetragonal ( $P4mm$ ) phases after poling as evident from the triplet nature of the both  $\{111\}_{pc}$  and  $\{200\}_{pc}$  compositions (Fig. 3). The characteristic superlattice peak of the  $R3c$  phase which was invisible in the XRD patterns of unpoled specimens of  $x = 0.20$  and  $x = 0.22$  (insets of

Fig. 3) becomes visible after poling. Our analysis therefore suggests that it is the poled  $x = 0.22$  (and not poled  $x = 0.20$ ) which mimics the conventional MPB compositions, such as that of PZT.

Based on this visual inspection, we first attempted Rietveld fitting of poled  $x = 0.22$  with  $R3c + P4mm$  model but the fit was not very satisfactory. A satisfactory fit was obtained only after considering a minor (11%) cubic phase [Fig. 10(a)]. Similarly, although the visual inspection suggests a rhombohedral structure for all poled specimens with  $x \leq 0.20$ , Rietveld fitting with single-phase  $R3c$  was found to be very unsatisfactory [Fig. 10(b)]. The fit improved remarkably after including a cubic phase in the structural model [Fig. 10(c)]. Following this, we fitted the patterns of the poled specimens in the range  $0 \leq x \leq 0.20$  with  $R3c + Pm-3m$  structure model (Fig. 11). The volume fraction of the cubic phase increased as

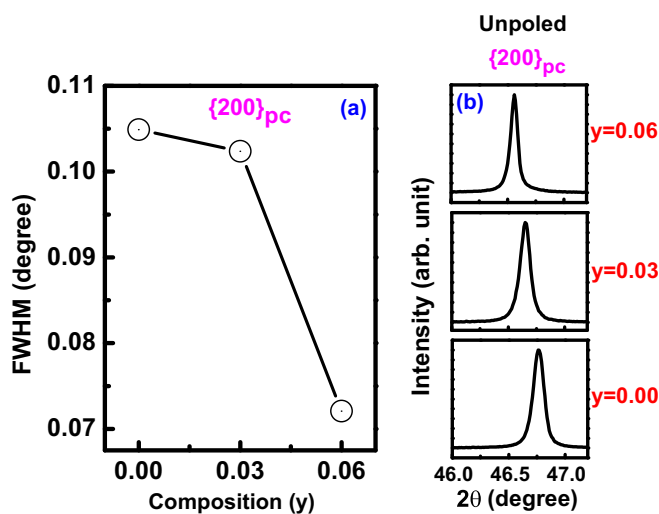


FIG. 6. (a) Composition dependence of the FWHM of the single Bragg profile  $\{200\}_{pc}$  of unpoled  $(1 - y)$ NBT- $y$  BT. (b) X-ray powder-diffraction Bragg profile  $\{200\}_{pc}$  of unpoled NBT –  $y$ BT specimens.

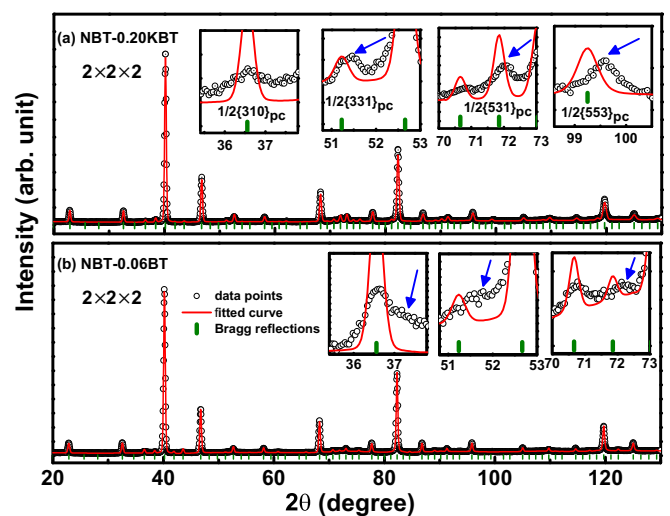


FIG. 7. Le Bail fitting of the neutron powder-diffraction pattern of two different NBT-based MPB systems (a) NBT-0.20KBT and (b) NBT-0.06BT with  $2 \times 2 \times 2$  cubic ( $Pm-3m$ ) supercell. The insets highlight the magnified peak misfits in the superlattice peaks (indicated by arrows).

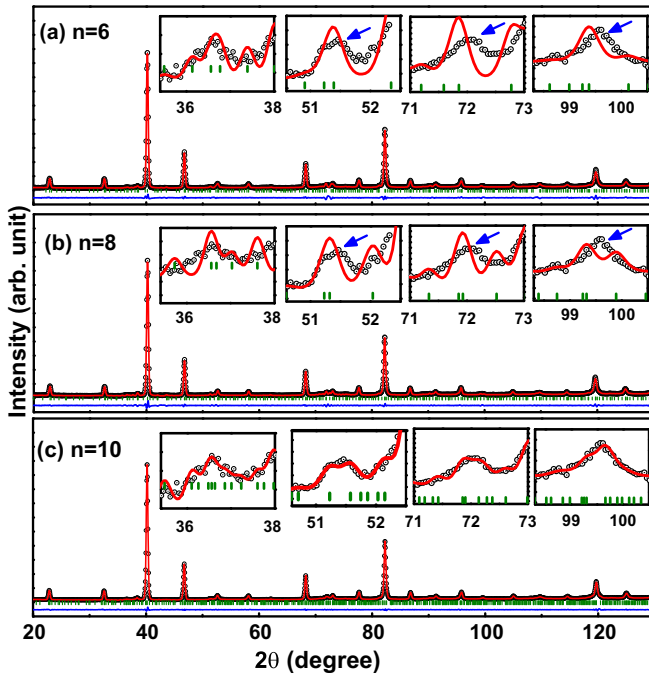


FIG. 8. Le Bail fitting of the room temperature NPD pattern of unpoled NBT-0.20KBT fitted with a  $\sqrt{2}a \times \sqrt{2}b \times nc$ -type cell with (a)  $n = 6$ , (b)  $n = 8$ , (c)  $n = 10$ . The arrows highlight the misfit regions near the superlattice peaks.

with increasing KBT concentration [Fig. 12(a)]. The rhombohedral lattice strain of the poled specimens measured in terms of  $(90^\circ - \alpha)$ , where  $\alpha$  is the rhombohedral angle decrease as the MPB is approached [Fig. 12(b)]. Interestingly, the maximum piezoelectric coefficient ( $d_{33}$ ) at  $x = 0.20$  is also the composition which exhibits maximum volume fraction ( $\sim 35\%$ ) of cubic phase [Fig. 12(c)]. As compared to the unpoled state, the FWHM of  $\{200\}_{pc}$  increased noticeably after poling for all the compositions  $x \leq 0.20$  [Fig. 12(d)], most likely due to the enhanced strain caused by switching of the ferroelectric-ferroelastic domains [51,61–63]. The strain caused by the switching of domains is more for the critical composition  $x = 0.20$  (MPB) in comparison to the lower

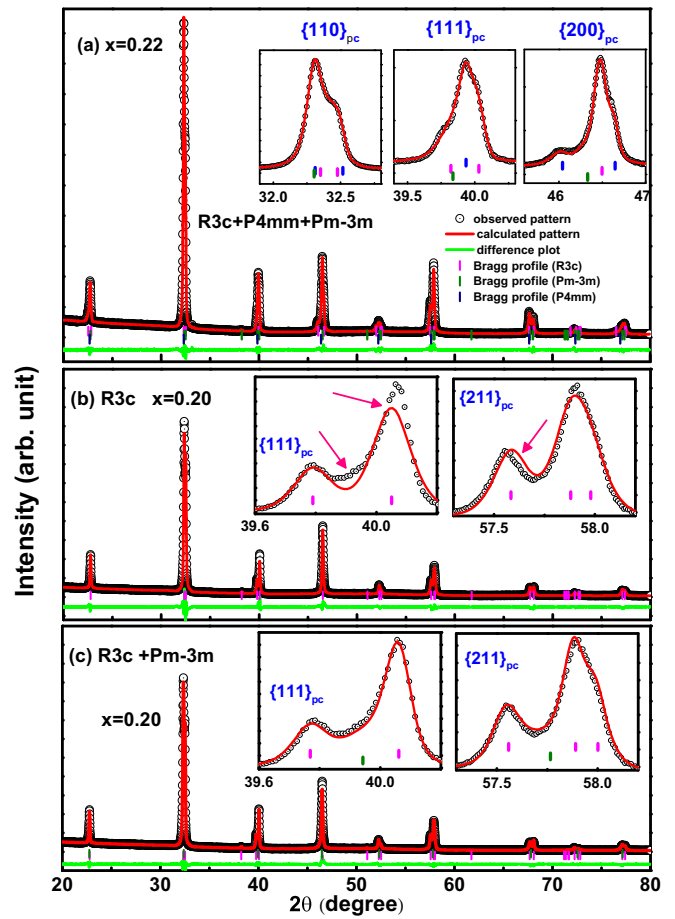


FIG. 10. (a) Rietveld fitted XRD pattern of poled NBT-0.22KBT sample, fitted with the  $R3c$  (43%) +  $P4mm$  (45%) +  $Pm-3m$  (12%) structural model. For the sake of direct comparison (b) and (c) show Rietveld fitted XRD pattern of poled NBT-0.20KBT with single-phase  $R3c$  and  $R3c + Pm-3m$  phases, respectively. Insets highlight some of the representative Bragg peaks, and arrows indicate misfit regions in (b) when an attempt to fit was made with single-phase  $R3c$ .

compositions [Fig. 12(d)] presumably due to enhanced propensity for domain switching near the MPB.

The NPD pattern of poled  $x = 0.20$  also shows remarkable changes. Consistent with the XRD pattern, several of the main Bragg profiles of the NPD pattern are split as per the rhombohedral distortion. Most remarkably, the weak superlattice peaks corresponding to the long-period modulation disappear after poling and are replaced by strong superlattice peaks characteristic of the  $R3c$  phase [Fig. 13(b)]. The slightly inferior resolution of the NPD data as compared to the XRD data precluded the requirement for considering a cubiclike phase, and a reasonable fit was obtained with single-phase  $R3c$  model. The suppression of the long-period modulation in the octahedral tilt after poling implies that poling has suppressed the short-ranged in-phase tilted regions in favor of the antiphase tilts. The requirement of the minor cubic phase to fit the XRD pattern of the poled specimen therefore is manifestation of the structural disorder the system retains after poling, due to the remanent localized islands of in-phase tilted regions amid the field-stabilized long-ranged  $R3c$  regions.

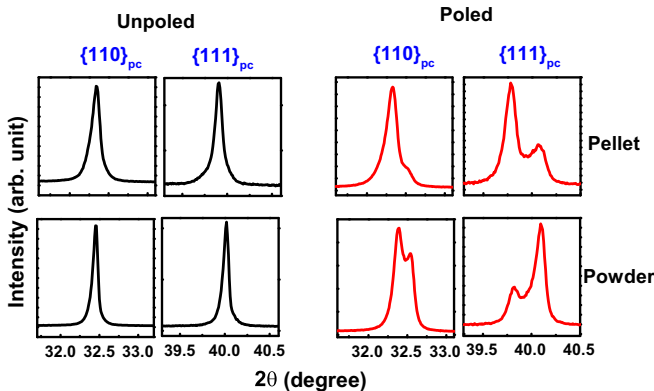


FIG. 9. XRD patterns of selected Bragg peaks for  $x = 0.20$  in unpoled and poled states from pellet as well as from fine powders in NBT- $x$ KBT.

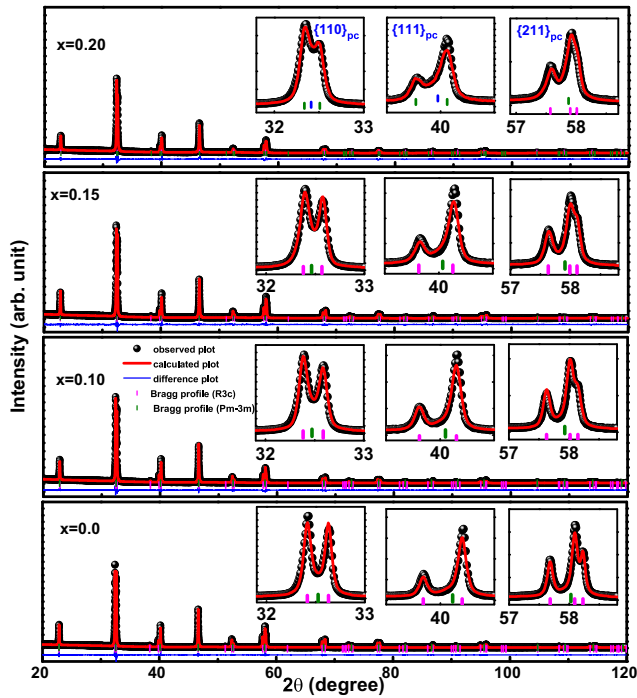


FIG. 11. Rietveld fitted XRD patterns of poled NBT -  $x$ KBT ( $x \leq 0.20$ ) compositions with  $R3c + Pm-3m$  model. Insets show representative Bragg profiles.

### E. Local structures: Raman spectroscopy

Raman spectroscopy is a powerful tool to probe structural features on short length scales [64]. In the present context, wherein XRD is incapable of revealing the nature of the ferroelectric phases accompanying the MPB in unpoled specimens, analysis of the vibration modes in the Raman spectrum can throw light on the structural evolution with composition on the local scale. The Raman spectra of  $(1-x)$ NBT- $x$ KBT are mainly centered in three regions [Fig. 14(a)]. We assign them as *A* band ( $100-200 \text{ cm}^{-1}$ ), *B* band ( $200-400 \text{ cm}^{-1}$ ), and *C* band ( $400-650 \text{ cm}^{-1}$ ). The mode in *A* band is associated with the Na/K-O vibration, in the *B* band with Ti-O vibration, and in the *C* band with vibrations involving oxygen displacements [65,66]. For convenience of labeling and following earlier reports [67], the peak in the range  $\sim 109 - 116 \text{ cm}^{-1}$  is labeled as  $E(\text{TO}_1)/E(\text{LO}_1)$  and  $130 - 150 \text{ cm}^{-1}$  by  $A_1(\text{TO}_1)/A_1(\text{LO}_1)$  mode. Distinct changes with composition can be noted in the shape of the *A* band ( $100-200 \text{ cm}^{-1}$ ) [Fig. 14(b)]. The  $A_1(\text{TO}_1)$  mode centered at  $140 \text{ cm}^{-1}$  appears to be symmetric in the composition range  $0 \leq x \leq 0.10$ . At  $x = 0.12$  an asymmetry develops due to appearance of an  $E(\text{TO}_1)$  mode on the low-wave-number side at  $112 \text{ cm}^{-1}$ . The intensity of the  $E(\text{TO}_1)$  mode grows with increasing KBT concentration [Fig. 14(e)]. At  $x = 0.17$ , the intensity of the  $E(\text{TO}_1)$  and the  $A_1(\text{TO}_1)$  modes are comparable, making the *A* band appear as a doublet [Fig. 14(b)]. For  $x \geq 0.20$ , the  $E(\text{TO}_1)$  mode dominates and there appears to be no further remarkable change in the Raman spectra with increasing  $x$ . The  $E(\text{TO}_1)$  mode represents the tetragonal ( $P4mm$ ) phase. Since the tetragonal distortions are not visible in the XRD patterns

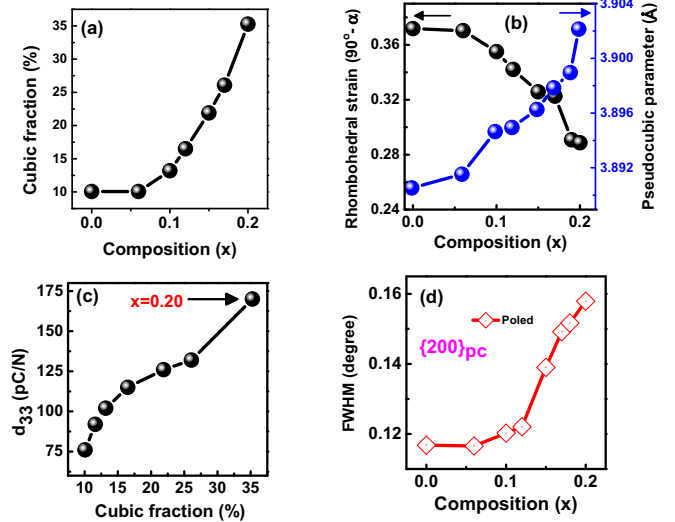


FIG. 12. (a) Composition dependence of the cubic fraction in the poled specimens of NBT -  $x$ KBT ( $x \leq 0.20$ ). (b) Composition dependence of the rhombohedral strain ( $90^\circ - \alpha$ ) and rhombohedral lattice parameter. (c) Correlation between piezoelectric coefficient ( $d_{33}$ ) and the cubic fraction (in poled specimens). The composition  $x = 0.20$  exhibiting the maximum retained cubic fraction shows the maximum piezoelectric coefficient, confirming that structural disorder assists in the enhancement of the piezoelectric response. (d) Composition dependence of the FWHM of the singlet Bragg profile  $\{200\}_{pc}$  of poled samples.

of the unpoled specimens, the tetragonal regions are short ranged.

There is a concomitant change in the shape of the *B* band as the MPB ( $x = 0.20$ ) is approached; a distinct peak at  $322.3 \text{ cm}^{-1}$  becomes visible for  $x \geq 0.20$  [Fig. 14(g)]. Interestingly this composition range ( $0.10 < x < 0.20$ ) is the same in which strain relaxation occurs [Fig. 4(b)]. The Raman spectra of unpoled  $x = 0.20$  and  $x = 0.22$  are nearly identical, suggesting a similarity in their local structures. A qualitative difference between the two compositions could be ascertained only in their poled state [Fig. 14(d)]. For  $x = 0.20$ , poling decreases the intensity of the  $E(\text{TO}_1)$  mode noticeably with respect to the intensity of the  $A_1(\text{TO}_1)$  mode [Fig. 14(f)]. This is consistent with the XRD results which confirm rhombohedral phase in poled  $x = 0.20$ . For  $x > 0.20$ , the changes in the relative intensity of the  $E(\text{TO}_1)$  and  $A_1(\text{TO}_1)$  modes before and after poling are not significant. Given that the XRD measurements suggest the structure of poled  $x = 0.22$  to be coexistence of  $P4mm$  and  $R3c$ , it appears that poling has merely increased the correlation lengths of both the ferroelectric regions  $P4mm$  and  $R3c$  as compared to that in their unpoled state. In contrast, poling has dramatically altered the ferroelectric state ( $P4mm + R3c$ ) of unpoled  $x = 0.20$  by suppressing the short-ranged tetragonal  $P4mm$  regions and transforming them to  $R3c$  regions.

## IV. DISCUSSION

The inherent positional disorder in NBT makes the MPB of both NBT-KBT and NBT-BT systems qualitatively

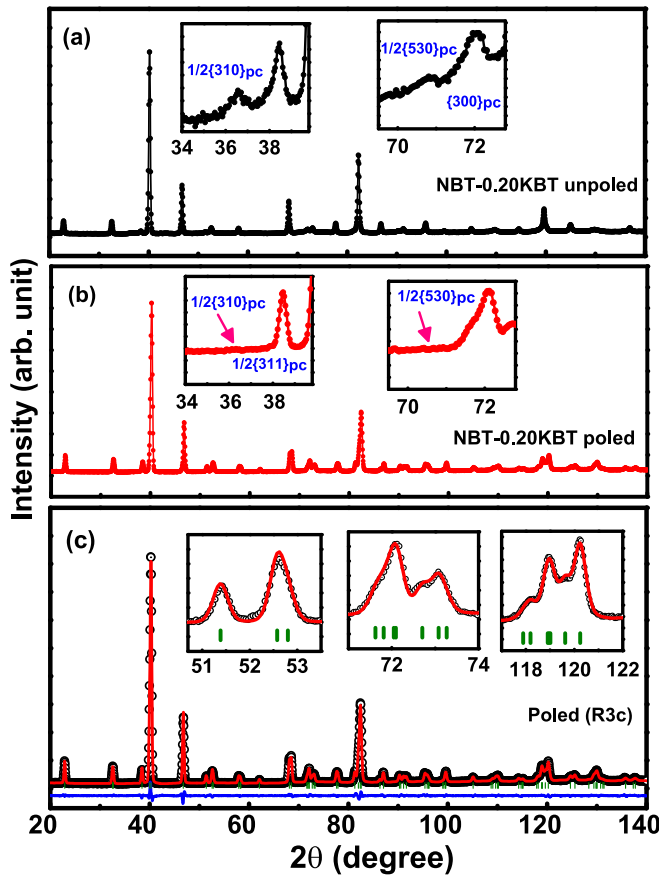


FIG. 13. Comparison of (a) unpoled and (b) poled neutron-powder-diffraction patterns of NBT-0.20KBT. In the insets, arrows indicate the superlattice peaks at the position of  $1/2(310)_{pc}$  and  $1/2(530)_{pc}$  which were prominent before poling (panel a) vanished after poling. (c) Rietveld plot of the room-temperature neutron-powder diffraction of poled NBT-0.20KBT fitted with rhombohedral ( $R3c$ ) structural model. The opened circles correspond to the observed pattern, the continuous (red) line between the data point is the fitted pattern, the vertical bars represent Bragg peak positions, and the difference plots are shown at the bottom of the figures (blue). The insets highlight fitted regions magnified.

different from the MPBs of the normal ferroelectrics such as the  $Pb(ZrTi)O_3$ ,  $Ba(Ti, Zr/Sn/Hf)O_3$ , and  $(K, Li)(Nb, Sb)O_3$ -based systems in the lead-free category. One way to highlight the difference can be from the viewpoint of how the depolarization temperature varies with composition. In normal ferroelectric-based MPB systems, the depolarization temperature is the Curie point itself and it exhibits a monotonous variation with composition. For example, the Curie point continuously decreases with increasing concentration of Zr in  $Pb(Ti_{1-x}Zr_x)O_3$ . The same is true for the  $Ba(Ti, Zr)O_3$  MPB system [12]. This decrease is a manifestation of the gradual decrease in the strength of the ferroelectric interaction (due to gradual reduction in the covalent character of the average B–O bond) [3,68,69]. In Fig. 15(a) we compare the composition variation of the Curie point of the  $Pb(Zr, Ti)O_3$  and the composition dependence of the depolarization temperature [Fig. 15(b)] of NBT-KBT. For reference sake we have shown a linear line joining the Curie points/depolarization

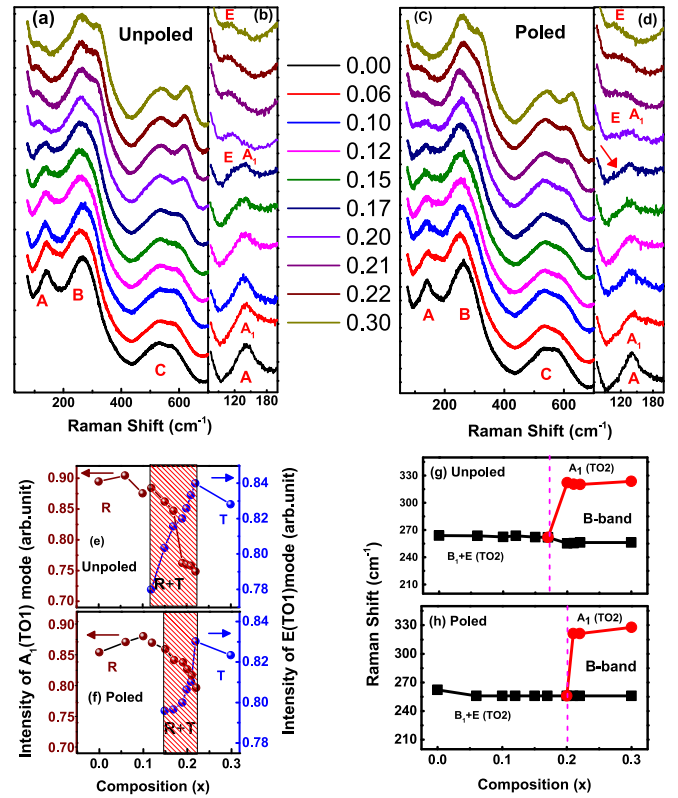


FIG. 14. (a) Composition evolution of the Raman spectra of unpoled NBT- $x$ KBT. (b) Magnified profile of the A band ( $100-190\text{ cm}^{-1}$ ). (c), (d) Corresponding spectra of poled specimens. (e), (f) Composition dependence of the intensity of  $E(TO_1)$  and  $A_1(TO_1)$  modes for unpoled and poled specimens, respectively. The frequency dependence of the Raman modes of the B band (as determined by multiline fits of the spectra) of unpoled and poled NBT- $x$ KBT are shown in (g) and (h), respectively. Splitting of  $B_1 + E(TO_2)$  mode starts from the composition  $x = 0.17$  for unpoled and starts from  $x = 0.20$  for poled.

temperatures of the extreme compositions [70,71]. The observed Curie points remain close to the linear line in the case of PZT. In contrast, the observed depolarization temperature is anomalously decreased ( $120\text{ }^\circ\text{C}$ ) with respect to the linearly extrapolated value ( $205\text{ }^\circ\text{C}$ ) at  $x = 0.20$ . This sharp dip in the depolarization temperature at the critical compositions of both NBT-KBT and NBT-BT [71–74] suggests an onset of another distortion near the MPB region which considerably weakens the ferroelectric interaction. In view of our NPD study and also the observations of others [49], it is evident that the special weakening of the ferroelectric character near the MPB of NBT-KBT and NBT-BT is caused by the considerably enhanced propensity of occurrence of the local in-phase tilted regions, which is incompatible with ferroelectric order.

de la Flor *et al.* have reported that the Raman mode near  $140\text{ cm}^{-1}$  softens as the depolarization temperature is approached in NBT-based piezoelectrics [75]. The modes near this frequency are therefore representative of the ferroelectric distortion in the system. The fact that the mode  $E(TO_1)$  at  $117\text{ cm}^{-1}$ , representative of the tetragonal ( $P4mm$ ) phase, becomes noticeable in the Raman spectrum of unpoled  $x = 0.12$  suggests that both the ferroelectric distortions,  $P4mm$

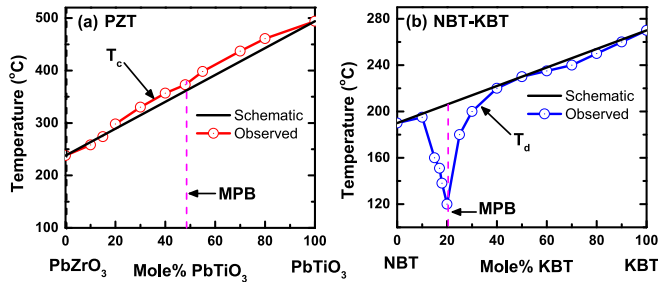


FIG. 15. (a) Composition dependence of the (a) Curie point of PZT [3], (b) depolarization temperature of NBT-KBT. The linear line joining the Curie points/depolarization temperatures of the extreme compositions serves as a reference to show the extent of deviation of observed values from that anticipated (based on the assumption that the Curie point/depolarization temperature varies linearly with composition). Note the dramatic dip in the depolarization temperature in NBT-KBT at  $x = 0.20$ .

and  $R3c$ , coexist in the unpoled specimens of  $0.12 \leq x \leq 0.22$ , on the small length scale [Fig. 14(e)]. As discussed above, the increased propensity of the local in-phase tilts precludes the development of long-range  $P4mm$  and  $R3c$  phases at the MPB. Previous studies have proved that NBT exhibits nanometer-sized in-phase octahedral tilt ( $a^0a^0c^+$ ) regions amid the relatively bigger-sized antiphase ( $a^-a^-$ ) tilt [37,38]. In most parts of the grains, the two tilt types are randomly stacked [38]. However, the occurrence of weak satellite peaks in diffuse scattering studies also points at the occasional occurrence of a long-period structural modulation (most probably sequentially stacked in-phase and antiphase tilts regions) with a periodicity  $\sim 40$  Å [41,76,60]. We argue that the inhomogeneous lattice strain observed by us in NBT is caused by the random stacking of the two different tilt types. Increased sequential ordering across the specimen volume can reduce the strain inhomogeneity in the system. This would require the system to have more volume fraction of the local in-phase tilted regions. The observation of superlattice peaks corresponding to the long-period modulation of octahedral tilt in unpoled  $x = 0.20$  proves that the system does prefer to increase the propensity of local in-phase tilted regions on approaching the MPB for minimizing the strain inhomogeneity the system inherited from its parent compound NBT. Thus, the approach towards the MPB from the NBT side is characterized by two features in NBT-based piezoelectrics: (i) interferroelectric  $R3c - P4mm$  instability, and (ii) overall enhancement in the in-phase tilt fraction. This explains the considerable weakening of the ferroelectric interaction near the MPB leading to a sharp dip in the depolarization temperature [Fig. 15(b)]. It also explains the absence of long-range  $P4mm$  and  $R3c$  correlations at the MPB in NBT-KBT and NBT-BT. The increased propensity for nonferroelectric (in-phase tilt) structural distortion for the sake of minimization of the random lattice strain makes NBT-based MPB piezoelectrics unique as compared to the classical normal ferroelectric-based MPB piezoelectric such as the PZT. In contrast to our case, the FWHM of the pseudocubic  $\{200\}_{pc}$  x-ray Bragg profile of PZT increases on approaching the MPB from the rhombohedral side [77]. The same observation was reported by other authors [78,79] confirming enhancement in

the inhomogeneous/random lattice strain as a precursor of the two-phase state. We anticipate that the same scenario would be applicable even in the NBT-KBT and NBT-BT had there been no dominating influence of the tilt disorder. In our case, the system first prefers to minimize the inhomogeneity in the lattice strain caused by the tilt disorder, even at the cost of inducing ferroelectric incompatible local in-phase octahedral tilts and weakens the stability of the ferroelectric state.

Our results also provide an opportunity to scrutinize the role of two ferroelectric phases near MPB in contributing towards the enhancement of piezoelectric response in ferroelectric solid solutions. The argument in support of the two-(ferroelectric) phase model for piezoelectricity enhancement relies on the mechanistic view that coexistence of two ferroelectric phases provides a large number of domain variants within and across the grains [7]. This helps in efficient poling and thereby improves the  $d_{33}$ . Our results do not seem to concur with this viewpoint since the poled composition  $x = 0.22$  which shows the coexistence of tetragonal and rhombohedral phases exhibits lower  $d_{33}$  than the neighboring poled composition of  $x = 0.20$  (Fig. 1) which does not show coexistence of ferroelectric phases after poling (Fig. 3). Both Raman and XRD results demonstrate that the long-range ferroelectric phase stabilized after poling  $x = 0.20$  is rhombohedral with some fraction of coexisting cubiclike phase. Given the view that the cubiclike phase is representative of polar-structural disorder present in the system, our results indicate that coexistence of long-range ferroelectric order with optimum disorder in poled specimens is more effective in increasing the piezoelectric response near the critical composition. This scenario is analogous to what has recently been reported in  $(1-x)\text{PbTiO}_3 - (x)\text{Bi}(\text{Zr}_{1/2}\text{Ni}_{1/2})\text{O}_3$  (PT-BNZ) [80]. In this case, the poled composition exhibiting the highest piezoelectric coefficient ( $d_{33} \sim 400$  pC/N) shows coexistence of tetragonal and cubic phases. These results indicate that interferroelectric instability and polarization rotation mechanism need not necessarily be the most important guiding factor in the rationale design of piezoelectric materials with large electromechanical response.

## V. CONCLUSIONS

We have addressed two important issues pertaining to morphotropic phase boundaries in  $\text{Na}_{0.5}\text{Bi}_{0.5}\text{TiO}_3$ -based piezoelectric systems. Investigating two important solid solutions, namely  $\text{Na}_{0.5}\text{Bi}_{0.5}\text{TiO}_3 - \text{K}_{0.5}\text{Bi}_{0.5}\text{TiO}_3$  and  $\text{Na}_{0.5}\text{Bi}_{0.5}\text{TiO}_3 - \text{BaTiO}_3$ , we show that (i) the parent compound NBT exhibits noticeable inhomogeneous/random lattice strain, and (ii) that the evolution of the system towards the MPB is primarily dictated by the necessity to minimize this strain. The system accomplishes this by increasing the volume fraction of (nonferroelectric) local in-phase octahedral tilt distortion and forming a sequential stack of antiphase and in-phase tilt resulting in the MPB composition exhibiting a long-period modulated phase on the global scale. We also establish that the composition exhibiting the maximum piezoelectric response is the one which shows coexistence of positional disorder along with a field-stabilized long-range ferroelectric order, and not the one exhibiting coexistence of rhombohedral and tetragonal ferroelectric

phases. Our study suggests that the increased propensity for the nonferroelectric compatible in-phase tilt makes NBT-based MPB systems distinctly different from the conventional MPBs by precluding the stabilization of long-range ferroelectric phases (in unpoled specimens) and anomalously lowering the depolarization temperature at the MPB.

## ACKNOWLEDGMENTS

R.R. thanks the Science and Engineering Research Board (SERB) of the Department of Science and Technology, Government of India for financial support (Grant No. EMR/2016/001457).

- 
- [1] K. Uchino, *Piezoelectric Actuators and Ultrasonic Motors* (Kluwer Academic, Boston, 1996).
- [2] W. Heywang, K. Lubitz, and W. Wersing, *Piezoelectricity: Evolution and Future of a Technology* (Springer, Berlin, 2008).
- [3] B. Jaffe, W. R. Cook, and H. Jaffe, *Piezoelectric Ceramics* (Academic, New York, 1971).
- [4] H. X. Fu and R. E. Cohen, *Nature (London)* **403**, 281 (2000).
- [5] D. Damjanovic, *J. Am. Ceram. Soc.* **88**, 2663 (2005).
- [6] Y. M. Jin, Y. U. Wang, A. G. Khachatryan, J. F. Li, and D. Viehland, *Phys. Rev. Lett.* **91**, 197601 (2003).
- [7] J. Y. Li, R. C. Rogan, E. Üstündag, and K. Bhattacharya, *Nat. Mater.* **4**, 776 (2005).
- [8] B. Noheda, D. E. Cox, G. Shirane, S.-E. Park, L. E. Cross, and Z. Zhong, *Phys. Rev. Lett.* **86**, 3891 (2001).
- [9] European Commission, Directive 2002/95/EC of the European Parliament and of the Council of 27 Jan. 2003 on the restriction of the use of certain hazardous substances in electrical and electronic equipment, Off. J. Eur. Union L37, 19 (2003).
- [10] European Commission, Directive 2011/65/EC of the European Parliament and of the Council of 27 Jan. 2003 on the restriction of the use of certain hazardous substances in electrical and electronic equipment, Off. J. Eur. Union L174, 88 (2011).
- [11] J. Rödel and J.-F. Li, *MRS Bull.* **43**, 576 (2018).
- [12] W. Liu and X. Ren, *Phys. Rev. Lett.* **103**, 257602 (2009).
- [13] D. S. Keeble, F. Benabdallah, P. A. Thomas, M. Maglione, and J. Kreisel, *Appl. Phys. Lett.* **102**, 092903 (2013).
- [14] D. Xue, Y. Zhou, H. Bao, J. Gao, C. Zhou, and X. Ren, *Appl. Phys. Lett.* **99**, 122901 (2011).
- [15] D. Damjanovic, A. Biancoli, L. Batooli, A. Vahabzadeh, and J. Trodahl, *Appl. Phys. Lett.* **100**, 192907 (2012).
- [16] M. Acosta, N. Khakpash, T. Someya, N. Novak, W. Jo, H. Nagata, G. A. Rossetti, Jr., and J. Rödel, *Phys. Rev. B* **91**, 104108 (2015).
- [17] K. Brajesh, K. Tanwar, M. Abebe, and R. Ranjan, *Phys. Rev. B* **92**, 224112 (2015).
- [18] K. Brajesh, M. Abebe, and R. Ranjan, *Phys. Rev. B* **94**, 104108 (2016).
- [19] M. Abebe, K. Brajesh, A. Mishra, A. Senyshyn, and R. Ranjan, *Phys. Rev. B* **96**, 014113 (2017).
- [20] A. Akbarzadeh, K. Brajesh, Y. Nahas, N. Kumar, S. Prokhorenko, D. Swain, S. Prosandeev, R. Walter, I. Kornev, J. Íñiguez, B. Dkhil, R. Ranjan, and L. Bellaiche, *Phys. Rev. B* **98**, 104101 (2018).
- [21] Y. Nahas, A. R. Akbarzadeh, S. Prokhorenko, S. Prosandeev, R. Water, I. Kornev, J. Íñiguez, and L. Bellaiche, *Nat. Commun.* **8**, 15944 (2017).
- [22] W. Ge, J. Li, D. Viehland, Y. Chang, and G. L. Messing, *Phys. Rev. B* **83**, 224110 (2011).
- [23] Y. Dai, X. Zhang, and G. Zhou, *Appl. Phys. Lett.* **90**, 262903 (2007).
- [24] Y. Saito, H. Takao, T. Tani, T. Nonoyama, K. Takatori, T. Homma, T. Nagaya, and M. Nakamura, *Nature (London)* **432**, 84 (2004).
- [25] T. Iamsasri, G. Tutuncu, C. Uthaisar, S. Wongsanmai, S. Pojprapai, and J. L. Jones, *J. Appl. Phys.* **117**, 024101 (2015).
- [26] I. Levin, I. M. Reaney, E.-M. Anton, W. Jo, J. Rödel, J. Pokorny, L. A. Schmitt, H.-J. Kleebe, M. Hinterstein, and J. L. Jones, *Phys. Rev. B* **87**, 024113 (2013).
- [27] R. Garg, B. N. Rao, A. Senyshyn, P. S. R. Krishna, and R. Ranjan, *Phys. Rev. B* **88**, 014103 (2013).
- [28] R. Garg, B. N. Rao, A. Senyshyn, and R. Ranjan, *J. Appl. Phys.* **114**, 234102 (2013).
- [29] G. D. Adhikary, D. K. Khatua, A. Senyshyn, and R. Ranjan, *Acta Mater.* **164**, 749 (2019).
- [30] C. Ma, H. Guo, and X. Tan, *Adv. Funct. Mater.* **23**, 5261 (2013).
- [31] B. N. Rao, D. K. Khatua, R. Garg, A. Senyshyn, and R. Ranjan, *Phys. Rev. B* **91**, 214116 (2015).
- [32] A. K. Kalyani, K. Brajesh, A. Senyshyn, and R. Ranjan, *Appl. Phys. Lett.* **104**, 252906 (2014).
- [33] B. Q. Ming, J. F. Wang, P. Qi, and G. Z. Zang, *J. Appl. Phys.* **101**, 054103 (2007).
- [34] B. N. Rao, R. Datta, S. S. Chandrashekar, D. K. Mishra, V. Sathe, A. Senyshyn, and R. Ranjan, *Phys. Rev. B* **88**, 224103 (2013).
- [35] B. N. Rao, L. Olivi, V. Sathe, and R. Ranjan, *Phys. Rev. B* **93**, 024106 (2016).
- [36] J. Kreisel, P. Bouvier, B. Dkhil, P. A. Thomas, A. M. Glazer, T. R. Welberry, B. Chaabane, and M. Mezouar, *Phys. Rev. B* **68**, 014113 (2003).
- [37] V. Dorcet and G. Trolliard, *Acta Mater.* **56**, 1753 (2008).
- [38] I. Levin and I. M. Reaney, *Adv. Funct. Mater.* **22**, 3445 (2012).
- [39] E. Aksel, J. S. Forrester, J. L. Jones, P. A. Thomas, K. Page, and M. R. Suchomel, *Appl. Phys. Lett.* **98**, 152901 (2011).
- [40] S. Gorfman and P. A. Thomas, *J. Appl. Crystallogr.* **43**, 1409 (2010).
- [41] A. M. Balagurov, E. Y. Koroleva, A. A. Naberezhnov, V. P. Sakhnenko, B. N. Savenko, N. V. Ter-Oganessian, and S. B. Vakhrushev, *Phase Transitions* **79**, 163 (2006).
- [42] T.-M. Usher, I. Levin, J. E. Daniels, and J. L. Jones, *Sci. Rep.* **5**, 14678 (2015).
- [43] B. N. Rao and R. Ranjan, *Phys. Rev. B* **86**, 134103 (2012).
- [44] T. Takenaka, K. Maruyama, and K. Sakata, *Jpn. J. Appl. Phys. Part 1* **30**, 2236 (1991).
- [45] R. Ranjan and A. Dviwedi, *Solid State Commun.* **135**, 394 (2005).
- [46] M. Otonicar, S. D. Škapin, M. Spreitzer, and D. Suvorov, *J. Eur. Ceram. Soc.* **30**, 971 (2010).
- [47] T. Takenaka, H. Nagata, and Y. Hiruma, *IEEE Trans. Ultrason. Ferroelectr. Freq. Control* **56**, 1595 (2009).

- [48] I. P. Pronin, N. N. Parfenova, N. V. Zaitseva, V. A. Isupov, and G. A. Smolensky, *Sov. Phys. Solid State* **24**, 1060 (1982) [*Fiz. Tverd. Tela* **24**, 1860 (1982)].
- [49] M. Otonicar, S. D. Škapin, and B. Jancar, *IEEE Trans. Ultrason. Ferroelectr. Freq. Control* **58**, 1928 (2011).
- [50] B. Narayan, J. S. Malhotra, R. Pandey, K. Yaddanapudi, P. Nukala, B. Dkhil, A. Senyshyn, and R. Ranjan, *Nat. Mater.* **17**, 427 (2018).
- [51] K. V. Lalitha, A. N. Fitch, and R. Ranjan, *Phys. Rev. B* **87**, 064106 (2013).
- [52] M. Hinterstein, J. Rouquette, J. Haines, Ph. Papet, M. Knapp, J. Glaum, and H. Fuess, *Phys. Rev. Lett.* **107**, 077602 (2011).
- [53] A. J. Goetzee-Barral, T.-M. Usher, T. J. Stevenson, J. L. Jones, I. Levin, A. P. Brown, and A. J. Bell, *Phys. Rev. B* **96**, 014118 (2017).
- [54] W. Zeng, X. Zhou, J. Chen, J. Liao, C. Zhou, Z. Cen, T. Yang, H. Yang, Q. Zhou, G. Chen, and C. Yuan, *Appl. Phys. Lett.* **104**, 242910 (2014).
- [55] M. Hoelzel, A. Senyshyn, R. Gilles, H. Boysen, and H. Fuess, *Neutron News* **18**, 23 (2007).
- [56] J. Rodrigues-Carvajal, FULLPROF. A Rietveld Refinement and Pattern Matching Analysis Program (Laboratoire Leon Brillouin (CEACNRS), Saclay, France, 2000).
- [57] P. B. Groszewicz, M. Gröting, H. Breitzke, W. Jo, K. Albe, G. Buntkowsky, and J. Rödel, *Sci. Rep.* **6**, 31739 (2016).
- [58] D. K. Khatua, A. Senyshyn and R. Ranjan, *Phys. Rev. B* **93**, 134106 (2016).
- [59] A. M. Glazer, *Acta Crystallogr., Sec. A* **31**, 756 (1975).
- [60] P. A. Thomas, S. Trujillo, M. Boudard, S. Gorfman, and J. Kreisel, *Solid State Sci.* **12**, 311 (2010).
- [61] D. A. Hall, A. Steuwer, B. Cherdhirunkorn, T. Mori, and P. J. Withers, *Acta Mater.* **54**, 3075 (2006).
- [62] D. K. Khatua, K. V. Lalitha, C. M. Fancher, J. L. Jones, and R. Ranjan, *Phys. Rev. B* **93**, 104103 (2016).
- [63] D. K. Khatua, K. V. Lalitha, C. M. Fancher, J. L. Jones, and R. Ranjan, *J. Appl. Phys.* **120**, 154104 (2016).
- [64] T. Steilmann, B. J. Maier, M. Gospodinov, U. Bismayer, and B. Mihailova, *J. Phys.: Condens. Matter* **26**, 175401 (2014).
- [65] J. Kreisel, A. M. Glazer, G. Jones, P. A. Thomas, L. Abello, and G. Lucazeau, *J. Phys.: Condens. Matter* **12**, 3267 (2000).
- [66] J. Kreisel, A. M. Glazer, P. Bouvier, and G. Lucazeau, *Phys. Rev. B* **63**, 174106 (2001).
- [67] M. K. Niranjan, T. Karthik, S. Asthana, J. Pan, and U. V. Waghmare, *J. Appl. Phys.* **113**, 194106 (2013).
- [68] S. Zhang, R. Xia, and T. R. Shrout, *J. Electroceram.* **19**, 251 (2007).
- [69] T. Yamamoto, *Jpn. J. Appl. Phys.* **35**, 5104 (1996).
- [70] S. C. Zhao, G. R. Li, A. L. Ding, T. B. Wang, and Q. R. Yin, *J. Phys. D* **39**, 2277 (2006).
- [71] B. N. Rao, A. Senyshyn, L. Olivi, V. Sathe, and R. Ranjana, *J. Eur. Ceram. Soc.* **36**, 1961 (2016).
- [72] K. Yoshii, Y. Hiruma, H. Nagata, and T. Takenaka, *Jpn. J. Appl. Phys., Part 1* **45**, 4493 (2006).
- [73] Y. Hiruma, K. Yoshii, H. Nagata, and T. Takenaka, *Ferroelectrics* **346**, 114 (2007).
- [74] F. Cordero, F. Craciun, F. Trequattrini, E. Mercadelli, and C. Galassi, *Phys. Rev. B* **81**, 144124 (2010).
- [75] G. de la Flor, T. Malcherek, S. Gorfman, and B. Mihailova, *Phys. Rev. B* **96**, 214102 (2017).
- [76] J. E. Daniels, W. Jo, and W. Donner, *JOM* **64**, 174 (2012).
- [77] Ragini, R. Ranjan, S. K. Mishra, and D. Pandey, *J. Appl. Phys.* **92**, 3266 (2002).
- [78] H. Yokota, N. Zhang, A. E. Taylor, P. A. Thomas, and A. M. Glazer, *Phys. Rev. B* **80**, 104109 (2009).
- [79] K. A. Schonau, L. A. Schmitt, M. Knapp, H. Fuess, R.-A. Eichel, H. Kungl, and M. J. Hoffmann, *Phys. Rev. B* **75**, 184117 (2007).
- [80] R. Pandey, B. Narayan, D. K. Khatua, S. Tyagi, A. Mostaed, M. Abebe, V. Sathe, I. M. Reaney, and R. Ranjan, *Phys. Rev. B* **97**, 224109 (2018).